

Synthesis and Crystallization of Precision ADMET Polyolefins Containing Halogens

Emine Boz and Kenneth B. Wagener*

The George and Josephine Butler Polymer Research Laboratory, Department of Chemistry, University of Florida, Gainesville, Florida 32611-7200

Anindya Ghosal, Riqiang Fu, and Rufina G. Alamo*

FAMU/FSU College of Engineering, Department of Chemical and Biomedical Engineering, and National High Magnetic Field Laboratory, Tallahassee, Florida 32310-6046

Received March 7, 2006; Revised Manuscript Received April 20, 2006

ABSTRACT: We report the synthesis and characterization of a series of precision polyethylene (PE) structures containing either a fluorine, chlorine, or bromine on each and every 19th carbon. The use of ADMET polymerization chemistry allows unprecedented control in the synthesis of these halogen containing PE derivatives, and results in the first bromine containing polyolefin with a precisely defined primary structure. Polymerization with Grubbs' first generation catalyst followed by hydrogenation by diimide reduction or Wilkinson's catalyst leads to these precise structures, which have been characterized by ^1H NMR, solution and solid state ^{13}C NMR, solid state ^{19}F NMR, IR, elemental analysis, TGA, DSC, AFM, and WAXD. The TGA data, coupled with elemental analysis, supply definitive proof of the structural composition through the observed thermal decomposition and release of exact masses of HX ($X = \text{F}, \text{Cl}, \text{or Br}$). In reference to analogous random copolymers, these precisely substituted polymers display sharper WAXD diffraction patterns, higher crystallinities and much narrower melting peaks, typical of a homopolymer-like crystallization. This crystallization behavior is supported by solid-state NMR based on the observed equivalence in the relative distribution of halogens between crystalline and noncrystalline regions. Extensive experimental data provide evidence for a crystalline state built on the basis of substitutional solid solutions. Lattice distortions caused by the accommodation of the substituent in the lattice render a change from orthorhombic to triclinic structures at a van der Waals atomic radius of the solute $> 1.6 \text{ \AA}$. The observed melting temperatures and enthalpies of fusion decrease dramatically with increasing volume of the substituent and scale proportionally to the van der Waals atomic radius in the halogenated series.

Introduction

Polyolefins are among the most important large volume polymers produced today.¹ Polyethylene (PE) has found use in such diverse areas as packaging, biomaterials, microelectronics, and protective coatings,² all of which depend on the tunable semicrystalline morphology of the polymer.³ Modification of the parent structure through halogen incorporation, as in the case of poly(vinyl chloride) (PVC) or poly(tetrafluorethylene) (PTFE),⁴ further extends the range of applications as a result of changes in polymer structure at all levels.^{5–7}

Ethylene–vinyl halide (EVH) copolymers also are of interest. Ethylene–vinyl chloride (EVC) copolymers offer improved thermal stability relative to PVC.⁸ Similarly, ethylene vinyl fluoride (EVF) polymers are of value, such as poly(vinyl fluoride) (PVF), poly(vinylidene fluoride) (PVF₂), and poly(ethylene-*alt*-tetrafluorethylene).⁹ Ethylene vinyl bromide copolymers¹⁰ and partially brominated polyethylene¹¹ are less well-known.

Synthesizing copolymer variants of common halogenated polyolefins can be challenging due to reactivity ratio issues present during copolymerization^{12,13} and due to the ineffectiveness of post polymerization attempts to produce well-defined structures.^{13,14} Of the various techniques that have been used to synthesize EVH copolymers, the simplest approach is halogenation of PE, a procedure which gives an irregular distribution of halogens along the polymer backbone. Further-

more, the properties of the resulting polymer are highly dependent on the structure of the PE used and the conditions employed for the halogenation.^{13,14} Another typical post-polymerization method is reductive dehalogenation,¹³ where chemical reducing agents such as tributyltin hydride are used to replace halogens with hydrogens, yielding materials that experience the same structural irregularities problematic in all post polymerization strategies. The direct free radical copolymerization of ethylene and vinyl halide comonomers yields copolymers containing numerous structural defects and consequent instability.⁸ Regardless of monomer ratios, the copolymers contain inordinately high vinyl contents as a result of reactivity ratio imbalances, a phenomenon that can only be slightly improved by use of γ -ray induced polymerization.¹⁵ Ziegler–Natta conditions have also been employed for copolymerization, although controlling the copolymer composition in this method has proven extremely challenging.¹²

Olefin metathesis chemistry offers an alternative synthetic route to such polymers, based on the development of well-defined late transition metal catalysts.¹⁶ Ruthenium catalyzed ring opening metathesis polymerization (ROMP) can yield EVC copolymers possessing well-defined structures.⁸ Acyclic diene metathesis polymerization (ADMET)^{17,18} has also been used for the synthesis of a precisely defined EVC polymer.¹⁹ With ADMET, variation in the monomer structure gives access to a broad range of precisely defined polymers, allowing direct correlation of structure–property relationships.²⁰ The ability of ADMET to produce PE structures with precisely placed pendant

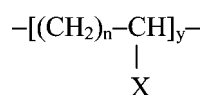
* Corresponding authors. E-mail: (K.B.W.) wagener@chem.ufl.edu; (R.G.A.) alamo@eng.fsu.edu.

groups is generating a wealth of structure/property data at the moment.

As has been known for decades now, the random incorporation of relatively small amounts (<10 mol %) of a structural irregularity in polyethylene (PE) generates copolymers possessing thermal properties that adhere to thermodynamic principles of phase transitions in two-component systems.^{21–23} The vast quantity of experimental data that exists unequivocally demonstrates that side groups such as ethyl, propyl, vinyl acetate, styrene, and others are not incorporated into the copolymer crystal lattice.²⁴ Their solid–liquid transition follows the basis of Flory’s equilibrium theory derived on the assumption of formation of a pure crystalline phase.²⁵ On the other hand, smaller side groups such as methyl, chlorine and oxygen can be partially incorporated into the crystalline lattice.^{22,23} A different partitioning of the side group has an important impact on the thermodynamic and physical properties of these copolymers. Thus, melting temperatures of random copolymers with Cl pendant groups and CH₃ branches are significantly higher than those of copolymers with matched compositions of side groups excluded from the crystal.²² The differences reflect the fraction of longer continuous crystallizable sequences present in the former type.

The analysis of the thermodynamic behavior of random ethylene copolymers with >~10 mol % branch points in the main chain is more complex. At this branching level, melting temperatures and degree of crystallinity usually deviate upward from the linear trends observed at the lower branching contents,^{21,26,27} and divergences are accentuated for copolymers with side groups that can be accommodated in the crystal.^{28,29} In reference to thermodynamic principles, concerns are raised about the actual branching distribution in highly branched systems and how close the crystallization behavior follows models based on selection of crystallizable sequences. On one hand, at large branching contents the usual temperature rising elution fractionation (TREF), crystallization fractionation (CRYSTAF) or NMR methods used to probe branching distributions either fail or become overwhelming in complexity.^{30,31} On the other hand, the decreased length of continuous methylene sequences may induce a different crystallization mode, as occasionally speculated²⁸ and in line with observations of a change in crystallographic packing with increasing comonomer content.^{28,29,32,33} Understanding the details of the crystallization behavior for these highly branched systems can only be accomplished via model polymers with well-defined microstructures. ADMET polymerization leads to polymers with precisely defined microstructures and, hence, to excellent models to study the crystallization behavior of highly branched ethylene copolymers.

ADMET polymerization followed by hydrogenation produces either the linear polymer chain or ethylene copolymer-type branched molecules that lack any branching composition distribution.^{17,19} This “clean polycondensation” chemistry is used here to produce a branched architecture characterized by the precise branch placement every “*n*” fixed methylene runs according to the following repeated structural unit:



The unique characteristics of these systems permit the study of ideal models of functionalized polyethylenes with precisely placed substituents in which *n* and *X* can be varied independently. They are models for polyethylenes with controlled hydrogen substitution.

We now report the ADMET synthesis and crystallization of a series of precision polyethylene structures containing fluorine, chlorine, and bromine located on each and every 19th carbon (*n* = 18) along the polymer backbone. Included in this study is the synthesis of the first bromine containing polyolefin with a precisely defined primary structure, demonstrating that the weaker carbon–bromine bond survives both the metathesis and hydrogenation chemistry employed. Not included is the comparative polymer containing iodine, as this precision polyolefin has eluded our efforts to create it. We continue to investigate synthetic routes to the iodine analogue copolymer, for it will become important in the final analysis of these halogenated polyolefins. For now, the synthesis and primary structure characterization of the fluorine, chlorine, and bromine containing polyolefins presented here delineates the opportunity for a detailed understanding of the effects of halogen incorporation in polyolefins.

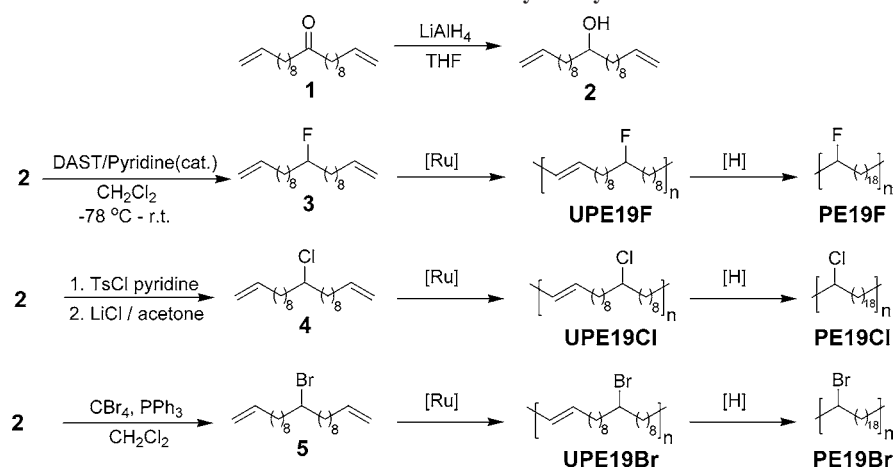
The effect of the substituent on the crystallographic packing is extracted using IR spectroscopy and wide-angle X-ray diffraction (WAXD), while the partitioning of the substituent between crystalline and noncrystalline regions is inferred from solid-state NMR spectroscopy and from the polymer’s thermal behavior. Since small atoms, such as oxygen and fluorine are expected to be accommodated in the all-trans polyethylene lattice, the systematic increase of van der Waals radius of the substituents in the series allows quantitative data of the degree to which the orthorhombic polyethylene lattice can tolerate atomic hydrogen substitution. The thermodynamic properties of these model systems will be directly correlated to substituent radius and bond lengths and will establish fundamental grounds for strategies to modify structural and thermal behavior of polyethylenes.

Results and Discussion

Synthesis. The synthesis of fluorine, chlorine, and bromine substituted EVH polymers with a halogen on each and every 19th carbon required the preparation of α - ω diene monomers, followed by ADMET polymerization and subsequent exhaustive hydrogenation as shown in Scheme 1. All three halogen-containing monomers were derived from a common ketone precursor **1**,³⁴ which was reduced to the alcohol **2**,³⁵ prior to halogenation. The fluorine monomer (**3**) was synthesized in good yield from **2** using diethylaminosulfur trifluoride (DAST). Chlorination was achieved by tosylation of **2** followed by nucleophilic displacement with LiCl, while the bromine monomer (**5**) was synthesized directly by action of CBr₄/PPh₃ on the alcohol **2**. Monomers **4**¹⁹ and **5** were then subjected to ADMET polymerization in the bulk using first generation Grubb’s catalyst.¹⁶ The fluorine monomer **3**, was polymerized in solution (methylene chloride) as this monomer is a solid as opposed **4** and **5**, which are oils. In a similar manner, the ketone starting monomer (**1**) was polymerized in toluene using first generation Grubb’s catalyst.

These unsaturated ADMET-EVH polymers were subjected to exhaustive hydrogenation to generate precision halogenated polyolefins. The nomenclature acronym used herein is UPE19X, where U indicates unsaturation and PE19X indicates a polyethylene backbone with a halogen substituent (X) on every 19th carbon. In the case of **UPE19F** and **UPE19Cl**, diimide reduction³⁶ gave clean conversion of the unsaturated polymer to the fully saturated polymer as evidenced by IR and NMR. Diimide reduction proved ineffective for **UPE19Br**. In this case it is likely that the presence of nucleophilic species in the hydrogenation mixture resulted in the displacement of the bromine, a mechanistic event facilitated both by the weaker

Scheme 1. Monomer and Polymer Synthesis

Table 1. Crystalline Data of Precision ADMET Polyolefins (PE19X) with General Structure $-(\text{CH}_2)_{18}-\text{CHX})_n-$

sample	atom ^a (X)	M_n 10 ⁻³ (g/mol)	M_w/M_n	packing cell	2θ (deg)				T_m (°C)	T_c (°C)	ΔH (J/g)	X_c^d (%)	vdW ^e (Å)	C-X ^f (Å)
					110	200	100	010						
PE	H	13.1	1.26	orthorh	21.64	24.02			133.0	115	238	83	1.2	1.09
PE19O	O	3.4 ^b	3.55	orthorh	21.43	23.28			134.7	120	106	60	1.52	1.2
PE19F	F	7.5 ^b	1.52	orthorh	21.23	23.60			127.5	113	207	57	1.47	1.35
PE19Cl	Cl	22.3 ^c	2.22	triclinic			19.10	22.47	72.7	63	105	50	1.75	1.78
PE19Br	Br	22.2 ^c	1.72	triclinic			19.20	21.95	61.5	43	55	40	1.85	1.95
PE19CH ₃ ¹⁷	CH ₃	11.3	1.90	triclinic			18.75 ^g	21.75 ^g	57	51	96	nd	2.0	1.54

^a Every 19th carbon. ^b Measured by GPC vs PE. ^c Measured by GPC vs PS. ^d Crystallinity from WAXS. Samples crystallized at 1 °C/min. ^e van der Waals radii. ^f C-X bond length. ^g -CH₃ group on and every 21st carbon.⁴³ ^h Melting and crystallization temperatures and heat of fusions correspond to samples crystallized and melted at 10 °C/min.

carbon bromine bond and the better leaving character of the bromine relative to chlorine and fluorine. Successful hydrogenation was achieved for UPE19Br as well as UPE19O (the polymer product of monomer 1) using Wilkinson's catalyst.³⁷ Polymer molecular weights were found to range from a M_w of 11 300–12 000 g/mol for PE19F and PE19O respectively (GPC vs PE) to 38 000–49 500 g/mol for PE19Br and PE19Cl respectively (GPC vs PS) as listed in Table 1.

Primary Structure Characterization. The primary structure for these well-defined halogenated polyolefins was established using a combination of ¹H NMR, ¹³C NMR, TGA (thermo-gravimetric analysis), IR spectroscopy, and elemental analysis. The precise structure of the polymers is supported by NMR, while TGA results prove the composition of the polymer through the clearly observed thermal decomposition and release of exact masses of HX (calculated HF = 7.0% and HBr = 23.5%, found HF = 7.3% and HBr = 22.7%), followed by catastrophic decomposition; as illustrated for PE19F and PE19Br in Figure 1 and previously observed for PE19Cl.¹⁹ The mass loss in all cases is in accord with the theoretically calculated value.

Figure 2 shows the IR spectra for thin films of the three halogenated polymers, data which also serve to support the expected primary structure. Here the absence of a peak at 967–969 cm⁻¹, corresponding to the out-of-plane C-H wag (γ_w) of an alkene,^{37,38} indicates complete hydrogenation of the polymer backbone. Further, the IR spectra support the presence of each of the expected halogens on the polymer backbone. For PE19F, the sharp peak at 1068 cm⁻¹ protruding from a broader underlying peak is characteristic of the C-F stretch.³⁹ The peaks observed at 611, 660, and 802 cm⁻¹ in PE19Cl are characteristic of C-Cl stretching vibrations,^{14,40} while for PE19Br, the peak at 612 cm⁻¹ is assigned to the vibrations of the C-Br bond.¹¹

These IR data also provide an insight into the crystalline structure of these precisely halogenated polymers. In this regard, the significant peaks are those found at ~720 and ~1470 cm⁻¹,

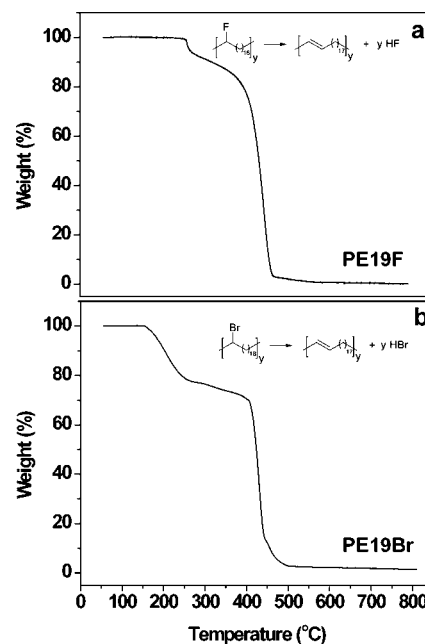


Figure 1. TGA for PE19F (a) and PE19Br (b) showing the loss of HF and HBr respectively, followed by catastrophic decomposition.

which correspond to the vibrational modes of the CH₂ sequences in PE analogues.¹⁴ For PE19F, the doublets observed at 721–730 and 1463–1472 cm⁻¹ are the same as observed in crystalline PE. The band at ~720 cm⁻¹ corresponds to long trans CH₂ sequences and the band at 730 cm⁻¹, is associated with the rocking vibrations of CH₂ sequences of five or more carbons.^{14,41} The IR spectra for PE19Cl and PE19Br are clearly different from those for the fluorinated analogue PE19F and pure PE, suggesting a distinct difference in the crystalline packing of these polymers. The Cl and Br precision polymers

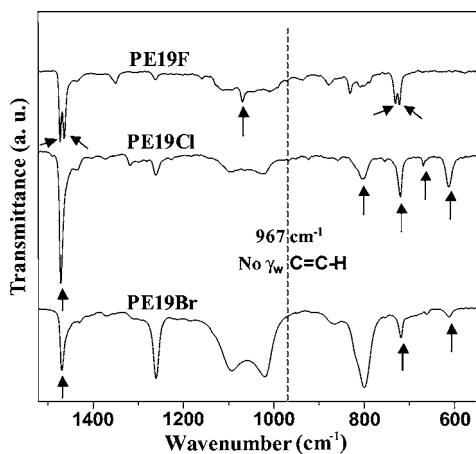


Figure 2. IR spectra for thin films of **PE19F**, **PE19Cl**, and **PE19Br** cast on KBr disks.

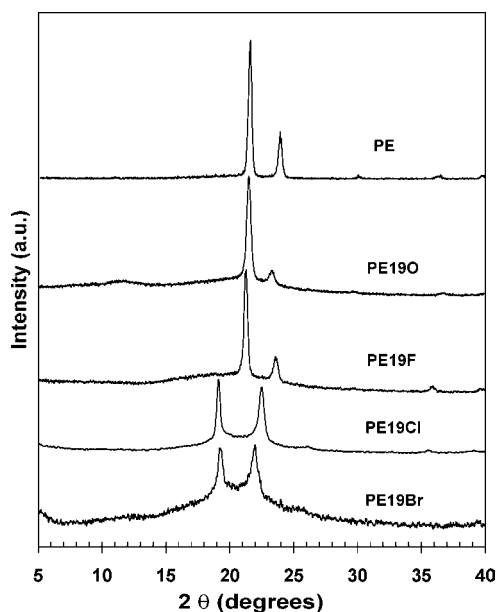


Figure 3. WAXD diffractograms of linear PE and ADMET precisely substituted polyethylenes slowly cooled from the melt at $\sim 1^\circ/\text{min}$. The pendant group ($X = \text{H}, \text{O}, \text{F}, \text{Cl}, \text{Br}$) is indicated in each pattern.

show a single peak rather than doublets at ~ 720 and ~ 1470 cm^{-1} , suggesting that these polymers possess similar crystalline features, yet differ from the fluorine and pure polyethylene counterparts. Both WAXD and solid-state ^{13}C NMR studies of the crystalline structure, presented in the following sections support these results.

WAXD. X-ray diffractograms of halogen containing ADMET samples cooled from the melt at $1^\circ/\text{min}$ are shown in Figure 3 together with the patterns of a matched PE19O (with a C=O group on each 19th carbon) and of a linear polyethylene narrow fraction in the same molecular weight range. It is at first evident that all samples display very sharp diffraction peaks, except for the broader pattern of the brominated material. In contrast, random ethylene copolymers with the same type of branching and with similar, and lower, branching levels are known to display much broader WAXD patterns.^{28,37,42} Hence, the sharp diffractograms of Figure 3 point to a homopolymer rather than copolymer-like crystallization behavior of these polyolefins. It is also evident that while substitution of hydrogen by O or F every 19th carbon does not alter the orthorhombic unit cell packing of the linear chain, substitution with a bulkier atom promotes formation of a different crystallographic phase.

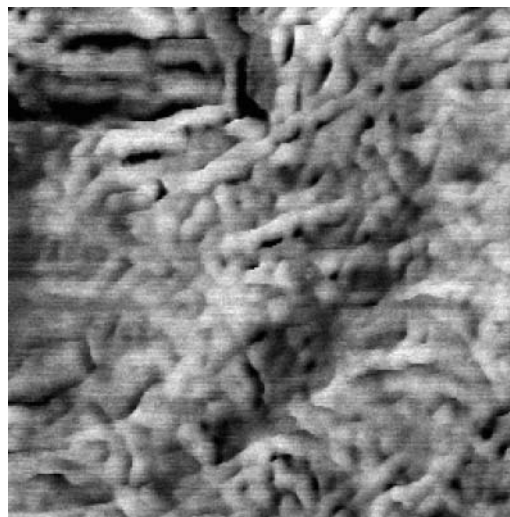


Figure 4. $2 \times 2 \mu\text{m}$ AFM phase image of melt crystallized **PE19Cl** with evident lamellar structure.

Diffraction peaks found at ~ 19 and $\sim 22^\circ$ for Cl and Br containing samples were also found in similar precisely placed methyl branched polymers and indexed as (010) and (100) diffractographic planes of a triclinic cell.⁴³ Therefore, in reference to this pattern, the diffractograms of **PE19Cl** and **PE19Br** are assigned to triclinic structures. Compared to the orthorhombic packing displayed by PE and polymers with F and O substitutions, the triclinic pattern is a degeneration in the scale of symmetry supporting previous speculation⁴³ that a reduced order is needed to facilitate minimum spatial requirements to accommodate the bulky Cl, Br, or CH_3 groups between adjacent molecules in the crystal. The triclinic pattern differs substantially from the single diffraction pattern observed for methyl branched polyethylenes or for ethylene vinyl chlorides with the same content of side groups but randomly distributed.^{28,32,33,37,42} In these systems single WAXD peaks were associated with defective orthorhombic or pseudohexagonal structures. Therefore, the progression of WAXD patterns of Figure 3 clearly evidence that both, *type and distribution* of the substituent, impact the chain ordering of branched or substituted polyethylenes at the most fundamental level.

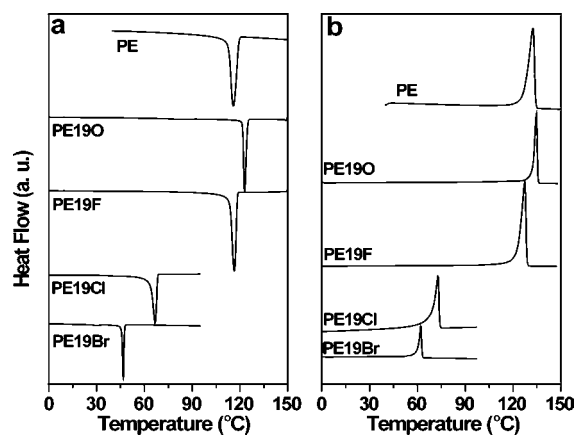
Evidence presented later by solid-state NMR of uniform partitioning of the side groups between crystalline and non-crystalline regions, precludes any correlation between the divergence in crystallographic features in the series and the content of substituent that is incorporated in the crystal. Furthermore, taking as a reference recent X-ray diffraction data on a similar precisely branched methyl polymer, unit cells that span over two repeating units (c axis $> 40 \text{ \AA}$) and crystallite thicknesses $> 100 \text{ \AA}$,⁴³ rule out any crystallization mode of these polymers based on selection of continuous methylene sequences between branches. The similar packing of Cl- and Br-containing polymers predicts an analogous behavior to the methyl branched sample that is evidenced by the 240 \AA crystal thickness obtained by atomic force microscopy (AFM) for melt crystallized **PE19Cl**, as shown in Figure 4. This value is well above the $\sim 23 \text{ \AA}$ thickness that corresponds to 18 all-trans methylene units and is in agreement with the participation of the substituent in the polymer crystal structure. Estimated thicknesses from the Scherrer equation⁴⁴ applied to the (110) and (100) planes of the orthorhombic and triclinic cells respectively, are also relatively large, with values of 270 (**PE19F**), 218 (**PE19O**), 268 (**PE19Cl**), and 191 \AA (**PE19Br**).

Table 2. Lattice Parameters from WAXD for Orthorhombic PE19X (X = H, O, F) Crystals

	packing cell	<i>a</i> (Å)	<i>b</i> (Å)	<i>c</i> (Å)	<i>V</i> (Å ³)	density (g/cm ³)
PE	orthorh	7.410	4.934	2.547	93.131	0.9983
PE19O	orthorh	7.643	4.937	2.547	96.098	0.9748
PE19F	orthorh	7.540	5.032	2.547	96.639	0.9802

The 2θ values of the diffraction peaks, together with other characterization data, are listed in Table 1 for the PE and ADMET precisely substituted polymers. Also listed are X van der Waals radii and C–X bond lengths. Inspection of these data allows evaluation of lattice expansions in reference to geometric constraints imposed by the solute X in the adjoining matrix. Compared to the unsubstituted polyethylene chain, the shift of 2θ (110) and 2θ (200) in the PE19F and PE19O patterns to lower angular values, reflects the expansion of the orthorhombic lattice due to an increase in both, van der Waals radius and bond length of C–F and C=O, respectively. Similarly, the increase in the spacing of the triclinic (010) plane from $2\theta = 22.47^\circ$ (3.96 Å) for PE19Cl to $2\theta = 21.95^\circ$ (4.05 Å) for PE19Br is also explained by the increased radius and bond length of the Br atom. Therefore, the angular shifts follow expectations from the significant incorporation of side groups in the crystalline structure. In addition, sharp diffraction peaks in most patterns point to a high correlation of diffractographic planes and, hence, to highly organized crystalline structures. Given the atactic character of the substitution,¹⁹ it appears that for the samples analyzed here, the orientation of the substituent with respect to the backbone chain has a negligible effect on the correlation between crystallographic planes. Calculated unit cell dimensions and densities of the orthorhombic lattices, for uniform distribution of F and O atoms, are listed in Table 2. Pertinent data for dimensions of the triclinic lattices could not be obtained since they would require observation of at least five independent WAXD reflections.⁴³

The diffractograms of Figure 3 also indicate that there is a significant amorphous region in these systems that increase with the bulkiness of the substituent. To estimate the degree of crystallinity from the diffractograms, the WAXD patterns obtained at 150 °C were scaled and subtracted from the room-temperature patterns. Crystallinity levels obtained are listed in Table 1 and range from 83% for PE to ~40% for PE19Br. In comparison, random ethylene copolymers with the same level of methyl branching or chlorine pendant groups (~5.3 mol %), display much lower levels (~25%) and less organized crystallinities.^{15,17,28} One can then conclude that the initial selection of long methylene sequences, present in the random system, over sequences containing for example Cl or Br substituents, imposes additional constraints in the topology of the remaining melt for gathering additional sequences with the required length to propagate crystallization. More specifically, in the random systems, the crystallization is primarily driven by the selection of continuous crystallizable sequences longer than a critical value, while shorter sequences remain uncrystallized. Clearly, the lack of branching distribution in ADMET polyethylenes with side groups on each and every 19th carbon, invokes a homopolymer-like crystallization with a driving force led by the accommodation of the side group in an all-trans backbone packing conformation. This crystallization mode explains the sharp diffractograms and, as illustrated in Figure 4, the lamellar character of the crystallites formed from polyethylenes with a relatively high content of side groups. Thus, while the melting behavior of the random samples is invariably broad, precisely substituted polymers melt sharply as clearly indicated by the

**Figure 5.** DSC exotherms (a) and endotherms (b) of linear PE and precisely substituted polyethylenes cooled from the melt at 10 °C/min and further heated at 10 °C/min.

melting thermograms of PE21CH₃ and the randomly distributed counterpart (with matched methyl content) in Figure 8 of ref 37. The change in crystallographic packing of random vs precisely placed methyl branched ADMET systems is also clear evidence of their different crystallization behavior.³⁷

The fact that precisely substituted ADMET polymers display relatively high levels of crystallinity suggest a crystalline state built on the basis of substitutional solid solutions.⁴⁵ In packing backbone sequences in all-trans conformation, substitution of a H for O, F, Cl, or Br on each and every 19th carbon, creates lattice distortions on levels proportional to the solute's van der Waals radius. As seen in Table 1, the orthorhombic lattice is preserved in this series up to a radius of ~1.6 Å while bulkier atoms cause large lattice distortions to the point that correlated symmetry between crystallographic planes is only found within a different phase with significantly larger dimensions.⁴⁶ In reference to the hydrogen, the discontinuity of isomorphous structures in this series occurs at a difference in van der Waals radius of ~30%. This is larger than the ~15% or lower difference usually quoted for formation of isomorphous metallic solid solutions,⁴⁵ but not unexpected, taking into account the chain connectivity of polymer molecules and the weaker covalent bonding.

Melting and Crystallization Behavior. A further insight into the unique crystallization mode of this family of precisely substituted polyethylenes is given by their crystallization and melting behaviors as measured by differential scanning calorimetry (DSC) shown in Figure 5. The sharpness of the crystallization and melting traces are typical of the behavior of low molecular mass homopolymers, and they contrast with much broader endotherms displayed by random ethylene copolymers of similar branching composition.^{15,22,37} Thus, thermodynamic features also point to a mechanism for ordering the precisely branched ADMET polymers that differs from a partitioning of sequences along the crystallization process, which is typical of the random behavior.^{23,26} In the latter, a richer melt in substituents is inevitable due to the chain's noncrystallizable short sequences; this feature leads to an inequality in partitioning of the substituent between the crystalline and noncrystalline regions. As a consequence, the composition of the melt coexisting with crystallites changes continuously during melting, leading to the broad endotherms usually observed in the random systems.^{21,26,47}

The peak melting temperatures decrease dramatically and proportionally to the van der Waals radius in the series of halogenated polymers, as seen in Figure 6, projecting a value

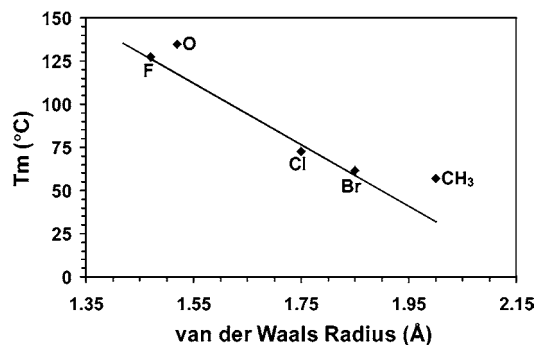


Figure 6. Peak melting temperatures of precisely substituted polyethylenes (PE19X) vs van der Waals radius of substituent (X). The linear regression was applied to halogenated samples.

of ~ 30 °C for the melting temperature of the iodine polymer with the same substituent pattern. We observe that for similar van der Waals radii, shorter bond lengths increase the melting temperature as evidenced by the ~ 7 degrees higher melting of **PE19O** compared to **PE19F**. Similarly, the melting temperature of **PE19CH₃**¹⁷ is higher than predicted from van der Waals radii arguments; due to a much shorter C–C bond length. The high heat of fusion of **PE19F** (Table 1) is associated with a high electronegativity of the F atom and its likelihood of increasing intermolecular secondary bonding compared to the other members of the series.

Clearly, the variation in crystallization and melting temperatures in this series is indicative of the degree to which each substitution perturbs the symmetry of the neighboring carbons in the lattice. Accommodation of the larger atoms must, by necessity, distort the all-trans ordering of vicinal intra- and intermolecular carbons resulting in a more defective structure and, as a consequence, in significantly altered thermodynamic data.

Solid-State NMR. Crystallographic and thermal properties of the series of precision substituted polyethylenes, such as the change and expansion of the unit cell and over 75 °C decrease in melting temperature with increasing van der Waals radius, were interpreted as the result from the need to pack in crystalline arrays continuous molecular segments that include the side groups. In this section, the inclusion of halogens in the crystalline regions is probed by direct solid-state NMR analysis of resonances belonging to or associated with the side group in ordered and disordered environments. Of the ADMET polymers investigated, **PE19F** is the best-suited candidate to reveal differences between crystalline and noncrystalline side groups. In this sample, direct polarization solid-state ¹⁹F NMR provides information on all fluorine atoms at high sensitivity while information via ¹³C NMR of the solid samples relies only on $\sim 1\%$ natural abundance of the ¹³C isotope.

The directly polarized ¹⁹F spectrum of **PE19F** obtained under high power ¹H decoupling (DD) and magic angle spinning (MAS) of 14 000 Hz is given in Figure 7a. The spectrum was obtained with a recycle time of 20 s to ensure complete F magnetization recovery. Paralleling the expected incorporation of a large fraction of F atoms in the crystalline regions, two distinctive resonances are observed associated with fluorine atoms in crystalline (–179.4 ppm) and noncrystalline (–181.9 ppm) environments. The integrated intensity associated with each resonance was extracted from a fit of the total intensity with two Lorentzian peaks, which led to a crystallinity of 56% in very good agreement with the 57% value obtained by WAXD for the same sample. Such a good correspondence is expected if **PE19F** crystallizes as a homopolymer with no discrimination

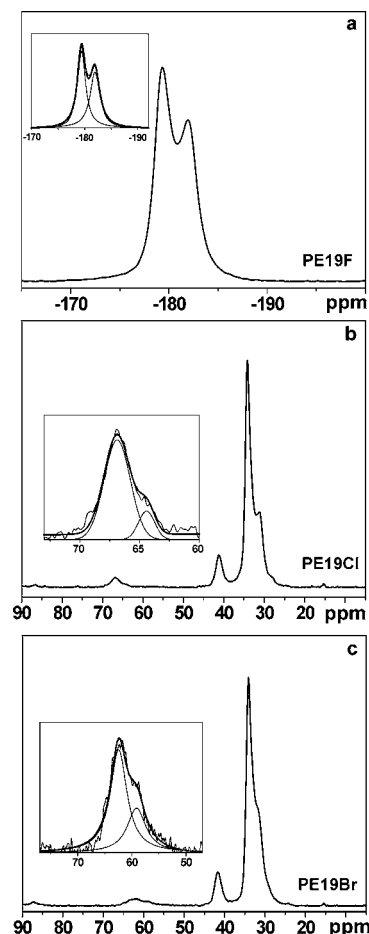


Figure 7. Fully relaxed ¹⁹F (a) and ¹³C NMR (b, c) DD/MAS spectra of **PE19F**, **PE19Cl** and **PE19Br** respectively. The fit of the ¹⁹F NMR spectral intensity with two Lorentzian components, corresponding to crystalline and noncrystalline F environments is shown in the inset. Also shown are expansions of the 50–80 ppm regions of the ¹³C NMR spectra fitted with two components for better distinction of CHCl and CHBr crystalline and noncrystalline resonances. [–(CH₂)₁₆–CH₂(β)–CH₂(α)–CHX–].

in the partition of the F side groups between the different phases of the crystalline structure. Contrasting with a clear difference in chemical shift between ordered and disordered F, the spin–lattice relaxation times (T_1^F) associated with both regions are very similar, 3.85 and 3.36 s respectively, denoting the lack of specific orientation of the F with respect to the backbone chain and the defective nature of this atom in the crystalline lattice.

Although the solid-state ¹⁹F NMR spectrum of Figure 7a evidences clearly the presence of F atoms in two different conformational environments, it does not provide direct quantitative information on the content of F in each region. This information is feasible via solid state ¹³C NMR by the correlation between CH and CH₂ carbons pertaining to crystalline and noncrystalline environments. Moreover, the ¹³C DD/MAS spectrum of **PE19F** was not recorded as the lower sensitivity of ¹³C observation added to our inability to decouple both ¹H and ¹⁹F simultaneously, will undoubtedly result in a broad featureless CH resonance.

Solid-state DD/MAS ¹³C NMR spectra were obtained for the other two halogen substituted polyethylenes of the series and are given in Figure 7, parts b and c, for **PE19Cl** and **PE19Br** respectively. Prior to acquisition of fully relaxed spectra, carbon spin–lattice relaxation times for CH, α CH₂, and crystalline CH₂ groups in both polymers were estimated as 1.5, 2, and 25 s respectively. Accordingly, fully relaxed single pulse spectra

of >2600 transients were collected at room temperature under MAS and high power ^1H decoupling using recycle times of 120 s. Small peaks observed at 15.3 ppm are associated with spinning sidebands. The main resonance centered at 34.1 ppm corresponds to crystalline CH_2 in the all-trans conformation and is shifted 1.3 ppm downfield in reference to the crystalline orthorhombic CH_2 resonance of linear polyethylene, which is centered at 32.8 ppm under the same field and experimental conditions. This shift points to a crystallization pattern for **PE19Cl** and **PE19Br** that differs from the orthorhombic symmetry as previously observed by WAXD. A correspondence with similar downfield shifts observed in solid *n*-alkanes that pack in a triclinic phase as compared to the *n*-alkane orthorhombic symmetry,⁴⁸ serves as additional indirect evidence of the triclinic packing of these polymers. By analogy to the spectrum of solid PE, the resonance at 31.5 ppm is assigned to noncrystalline CH_2 carbons and by comparison to the spectrum recorded in solution, peaks centered at 41.2 and 41.4 ppm and at 67 and 62.5 ppm are assigned to α CH_2 and CH carbons of **PE19Cl** and **PE19Br**, respectively. The chemical shift for the β CH_2 is mostly hidden beneath the 31.5 ppm resonance of the amorphous CH_2 carbons.

As previously indicated, the peak corresponding to the CHX carbon is ideal for monitoring the partitioning of Cl and Br atoms between crystalline and noncrystalline regions. For this purpose the information from the CHX resonance is useful when both phases contain a sufficiently large number of CHX groups to overcome the low sensitivity nature of ^{13}C detection, and when crystalline and noncrystalline phases display a resolved difference in their CHX chemical shift. An additional constraint to acquire spectra with high signal/noise ratio in our samples was the small quantities of ADMET polymers available for these experiments (~35 mg). The spectral region associated with the CHX resonance is expanded in the inset of Figure 7, parts b and c. Both consist of two largely overlapping resonances centered at 66.9 and ~64 ppm for **PE19Cl** and at 62 and 59 ppm for **PE19Br**. In consonance with the resonances observed in **PE19F** in Figure 7a, the CHX observed resonances indicate that at least two populations of methine carbons with significantly different conformations are present in crystalline PE19X polymers. Small protrusions in the downfield wings of the crystalline CHX resonance are attributed to a high noise level from the small quantities sampled. The contribution from the interface will be buried within the crystalline and noncrystalline CHX resonances. Because the difference in chemical shift and the ratio of peak heights of these two resonances are very similar to the values of crystalline (34.1 ppm) and noncrystalline (31.5 ppm) CH_2 peaks, both CHX resonances are assigned to crystalline methine (66.9, 62 ppm) and noncrystalline methine (64, 59 ppm) carbons. The observed chemical shifts for crystalline and noncrystalline CHCl in Figure 7b are identical to the values reported by Tonelli et al. in a study of the structure of ethylene–vinyl chloride copolymers using CP/MAS techniques.⁴²

From the integrated intensities of the combined (crystalline and noncrystalline) CHX resonances and the intensity of α CH_2 resonance (~41.0 ppm) relative to the CH_2 resonances (34.1 and 31.5), contents of chlorine and bromine of 5.4 ± 0.3 and 5.3 ± 0.2 mol % are calculated, respectively. These values match the content of halogen in the molecule from the primary structure (5.3 mol %) and demonstrate the quantitative nature of the DD/MAS spectrum. In other words, all types of carbons of **PE19Cl** and **PE19Br** were relaxed after the 120 s delay. Since both CH_2 and CHX carbons have very similar distributions

Table 3. $T_{1\rho}^{\text{H}}$ Estimations from Two-Component Fits for PE19X (X = H, F, Cl, Br), with Values in ms

sample	fast	slow
PE	2	25
PE19F	1.8	24
PE19Cl	3.8	6
PE19Br	2.2	8

in amorphous and crystalline environments, from the equivalence in the corresponding intensity ratios, we conclude that chlorine and bromine groups must be uniformly distributed between the phases. Upon crystallization there is no discrimination for the partitions of CHX units between crystalline and noncrystalline regions. In contrast, the DD/MAS spectrum of a randomly distributed ethylene–vinyl chloride with similar chlorine content displayed much broader resonances and no distinction between crystalline and amorphous CHCl carbons.⁴² In the random copolymer at least 20% of the chlorines were estimated to be included in the crystal.

The distribution of side groups among the different phases of the semicrystalline structure was also probed by additional cross-polarized (CP) with MAS NMR experiments that isolate the spectra of the crystalline regions.^{49,50} Resonances in the crystalline spectra that are associated with the methine carbon or carbons adjacent to the methine group allow direct quantitative data on the content of these groups in the crystalline regions and, hence, on the partitioning of the side groups. As mentioned in the experimental part, the CP method used here for isolating the crystal spectra is based on differences in $T_{1\rho}^{\text{H}}$ of crystalline and noncrystalline regions. These values were estimated for the more intense ~34 ppm peak and are listed in Table 3 for the linear and three halogenated polymers. All the samples display a fast relaxing component, 2 ms < $T_{1\rho}^{\text{H}}$ < 4 ms, and a slower one ($T_{1\rho}^{\text{H}}$ > 6 ms), associated with the noncrystalline and more rigid crystalline phases, respectively. Owing to a modest contrast in crystalline and noncrystalline proton mobility for **PE19Cl** and **PE19Br** in the frequency level at which $T_{1\rho}^{\text{H}}$ is active, a 5 ms ^1H spin locking filter was applied for these two polymers prior to CP, and a longer one (7 ms) was used to filter most of the noncrystalline regions of **PE19F**. Consequently, crystalline spectra would be more strongly weighted after the filter. In addition to this filter, to further null or decrease the contribution of the noncrystalline carbons, a fraction of the unfiltered CP spectra (shown in Figure 8a) is subtracted from the spectrum generated with spin locking.^{49,50} The scaling factor for subtraction is chosen as the largest number that leaves no regions with negative intensities in the spectral region between 10 and 120 ppm. The resulting crystalline spectra are shown in Figure 8b and the corresponding observed chemical shifts for crystalline carbons in the halogenated series are listed in Table 4.

Unfiltered CP MAS spectra, shown in Figure 8a reveal an increase of the intensity of the amorphous CH_2 resonance (~31 ppm) with the size of the substituent, thus reflecting a decrease of crystallinity from **PE19F** to **PE19Br** in the series, in consonance with the WAXD data. Also of interest is the chemical shift corresponding to crystalline CH_2 of **PE19F**, observed at 33.1 ppm, a value that is very close to the all-trans orthorhombic linear polyethylene. This correspondence in chemical shifts confirms that **PE19F** maintains the orthorhombic packing of the PE chain.

Resonances of carbons associated with the substituents are still observed in the filtered crystal spectra (Figure 8b) even after subtraction of most of the amorphous components. These include the methine, the α CH_2 (~40 ppm) and the β CH_2 (observed at 28.6 ppm for **PE19F**, at ~31.0 ppm for **PE19Cl**

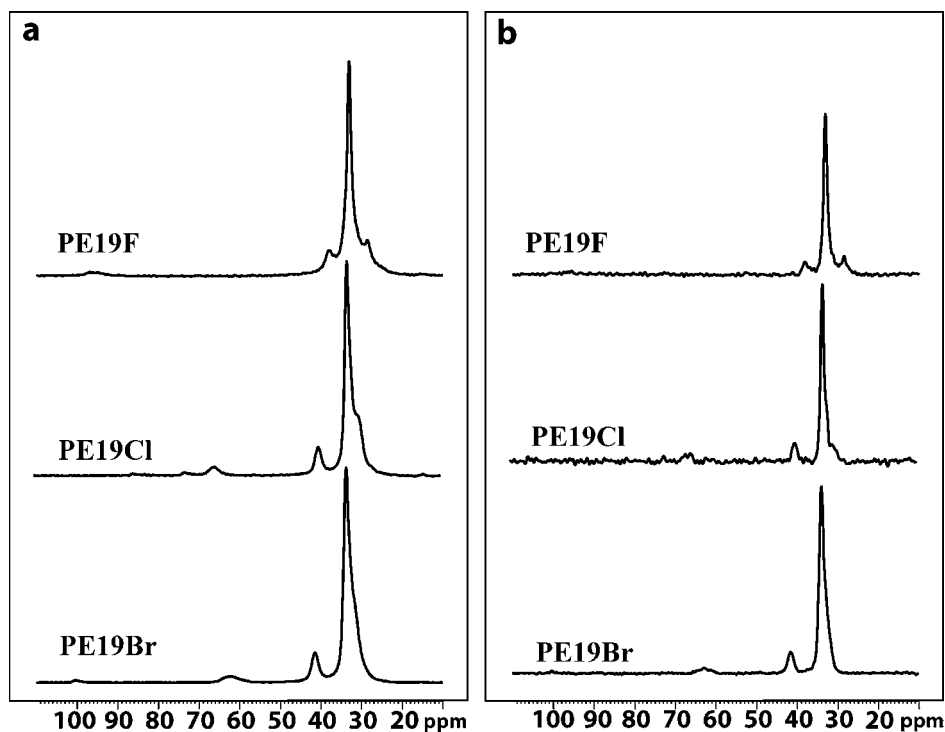


Figure 8. (a) ^{13}C NMR CP MAS spectra and (b) ^1H spin locking (crystalline) spectra of precision PE19X (X = F, Cl, Br) polyolefins.

Table 4. ^{13}C NMR Chemical Shifts for Crystalline Carbons of PE19X Precision ADMET Polyolefins (X = F, Cl, Br) and Concentration of X Groups in the Crystal

sample	chemical shift (ppm)				concentration of X in crystal (mol %) ^a		
	CH ₂ (PE-like)	α CH ₂	β CH ₂	CHX	from α CH ₂ intensity	from β CH ₂ intensity	from CHX intensity
PE	32.8						
PE19F	33.1	38.1	28.6	97 ^b	5.0	5.8	4.5
PE19Cl	34.1	41.0	~31	67	5.2	5.8	5.5
PE19Br	34.1	41.5	NO ^c	62.5	5.0		4.7

^a Calculated from ratio of integrated intensities in the crystalline spectra (Figure 8a). ^b Broad resonance. ^c Not Observed.

and buried within the main CH₂ resonance in the spectrum of PE19Br). Observation of these resonances confirms that all the types of halogen side groups are incorporated in the crystalline regions of these systems. This assertion is at variance with recent predictions from molecular dynamics (MD) simulations of the crystallization process of precisely placed methyl and chlorine side groups,⁵¹ yet it agrees with more abundant qualitative data, estimated from WAXD and DSC, for the random systems^{52–55} and precisely placed methyl branched polymers⁴³ which indicated that all types of side groups of interest here are incorporated in the crystal lattice.

The resolved character of relatively sharp α CH₂ resonances and the resonance associated with the CHX in the crystalline spectra allow us to integrate these lines against the integrals of the main peaks and, thus, deduce the concentration of F, Cl, and Br groups in the crystal. These data are also listed in Table 4. Accounting for the larger experimental error associated with integration of broad CHX resonances, the values obtained for the concentration of halogen in the crystal from any of the resonances associated with the side groups are very similar to the concentration of halogen in the chain (5.3 mol %). Therefore, analyses of CP MAS spectra confirm the results obtained from the DD/MAS spectrum of PE19F, PE19Cl, and PE19Br. They also confirm the uniform distribution of the halogen in the

semicrystalline structure and thus, the homopolymer crystallization behavior of these systems.

Conclusions

The synthesis and unique crystallization behavior of a series of precisely substituted polyolefins, with halogens (F, Cl, Br) or ketone groups on each and every 19th carbon, has been described, with synthesis of the precise, bromine-containing polymer (PE19Br) proving to be most challenging. Difficulties in isolating PE19Br were overcome via use of mild hydrogenation conditions using Wilkinson's catalyst. The very sharp diffraction patterns observed by WAXD and the narrow melting and crystallization peaks found by DSC for these polymers conform with a homopolymer-like crystallization. These observations contrast with much broader diffraction and melting peaks observed in ethylene copolymers with matched concentrations of randomly distributed side groups. In reference to the random copolymers, precisely substituted ADMET polymers display relatively high levels of crystallinity, as measured by WAXD, and a crystalline state built on the basis of substitutional solid solutions. The accommodation of O, F, Cl, or Br groups in the crystal creates lattice distortions on levels proportional to the solute's van der Waals' radius. The magnitude of the distortions are such that the PE orthorhombic lattice is only preserved up to a radius of ~ 1.6 Å (F, O substituents). Accommodation of bulkier substituents (Cl, Br) degenerates the correlated symmetry to a triclinic lattice with significantly larger dimensions. Direct solid-state ^{19}F and ^{13}C NMR investigations of the crystalline and noncrystalline regions evidence a uniform partitioning of all of these substituents between the different phases. While crystallization of the random type is led by the selection of long crystallizable sequences, in these precision polyolefins it is governed by the accommodation of the side groups into the crystal. As such, both *type and distribution* of the substituent impact the chain ordering of branched and substituted polyethylenes at the most fundamental level.

Experimental Section

Chemicals. Chemicals were purchased from the Aldrich Chemical company and used as received unless noted. Grubbs' first generation ruthenium catalyst, (bis(tricyclohexylphosphine)benzylidene)ruthenium(IV)dichloride, was purchased from Strem Chemical and stored in an argon filled drybox prior to use. Wilkinson's rhodium catalyst RhCl(PPh₃)₃ was purchased from Strem. Methylene chloride and *o*-xylene were distilled over CaH₂. PE (*M_n* = 13.1 kg/mol, PDI = 1.26) was obtained from the Societe Nationale des Petroles d'Aquitaine (SNPA).

Instrumentation. Solution ¹H NMR (300 MHz) and ¹³C NMR (75 MHz) spectra were recorded on a Varian Associates Gemini 300, VXR 300 or Mercury 300 spectrometer. All chemical shifts for ¹H and ¹³C NMR were referenced to residual signals from CDCl₃ (¹H = 7.27 ppm and ¹³C = 77.23 ppm) with an internal reference TMS 0.03% v/v. High-resolution mass spectral (HRMS) data were obtained on a Finnegan 4500 gas chromatograph/mass spectrometer using the electron ionization (EI) mode. Elemental analyses were carried out by Atlantic Microlabs Inc., Norcross, GA.

The GPC measurements for samples in THF were taken on a Waters GPCV 2K instrument. Samples were run with HPLC grade THF at 40 °C on Water StyragelHR 5E columns relative to polystyrene standards. Polymer molecular weights reported vs polyethylene standards were measured using a Waters Associates 150C high-temperature gel permeation chromatograph equipped with three Polymer Laboratories mixed bed Type B columns and an internal DRI detector. The mobile phase was BHT-inhibited 1,2,4-trichlorobenzene (135 °C, flow rate 1.0 mL/minute, typical sample concentration 2 mg/mL).

IR data was obtained using a Perkin-Elmer Spectrum One FTIR outfitted with a LiTaO₃ detector. Measurements were automatically corrected for water and carbon dioxide. Thermogravimetric analysis (TGA) data was obtained with a Perkin-Elmer 7 series thermal analysis system. The TGA samples (2–5 mg) were heated from –10 °C to 800 °C at 10 °C/min. Melting and crystallizations were obtained at 10 °C/min in a Perkin-Elmer differential scanning calorimeter DSC-7 with Pyris software under nitrogen flow and calibrated with indium.

WAXD diffractograms were collected at room temperature on samples crystallized from the melt at ~ 1 °C/min using a slit collimated Siemens D-500 diffractometer in a 2θ range between 5 and 40° with a step size of 0.02°. The instrument was calibrated for *d* spacing with a standard polished piece of polycrystalline quartz, and the film thickness was offset using shims. The diffractogram of molten polyethylene, used to estimate the degree of crystallinity, was collected at 150 °C on a Siemens D500 with an attached Anton Paar HTK high-temperature head.

DD/MAS solid-state ¹⁹F NMR spectra were obtained in a Bruker DRX 600 MHz spectrometer operating at 600.13 and 564.68 MHz for ¹H and ¹⁹F, respectively, under MAS frequency of 14 000 Hz and a decoupling power for ¹H of 71 kHz. Spin–lattice relaxation times were obtained via inversion recovery using ¹⁹F 90 and 180° pulse lengths of 2 and 4 μs, respectively. Chemical shifts were quoted with respect to the ¹⁹F isotropic signal of flufenamic acid (COOH–C₆H₄–NH–C₆H₄–CF₃) at –61.5 ppm as external reference.

¹³C NMR spectra of the solid polymers were obtained in a Bruker DMX300 spectrometer operating at 75.5 MHz for ¹³C and at 300.2 MHz for ¹H. The experiments for both types of solid-state NMR were conducted at room temperature using a Bruker solid-state probe for 4 mm rotors under a MAS frequency of 4000 Hz. The small quantities (<100 mg) available for these polymers were placed in the center of the zirconium rotors and the empty spaces filled with fine paper tissue or Teflon tape. The nutation frequencies associated with the ¹³C and ¹H radio frequency fields in the CP experiments were 62 kHz for both isotopes. The ¹H nutation frequency applied for decoupling was 83 kHz. Two different types of ¹³C NMR spectra were collected under high power ¹H decoupling, single pulse spectra with recycle delays sufficiently long to fully recover the magnetization of carbons in amorphous and

crystalline environments and ¹H–¹³C cross-polarization combined with MAS (CP MAS) spectra. Contact times for cross-polarization were 0.5–0.7 ms. Fixing the CP time and varying a proton spin locking pulse length, prior to cross-polarization, enables estimation of rotating-frame relaxation times, *T*_{1ρ}^H, for the protons. Values of *T*_{1ρ}^H for crystalline and amorphous regions, usually very different, can be used to filter the amorphous phase prior cross-polarization. The procedures have been detailed in previous works.^{49,50} Chemical shifts were measured with respect to tetramethylsilane at 0 ppm and using glycine's carbonyl carbon at 173 ppm as external reference. All peak fit analyses were carried out using the software GRAMS from Galactic Corp.

AFM images were obtained using the environmental JEOL 4210 scanning probe microscope operating under ambient conditions. Topographic and phase images were simultaneously collected in noncontact AC mode at 256 × 256 standard resolution using Olympus single side coated silicon cantilevers with resonant frequency at ~300 kHz.

Synthesis. Heneicosa-1,20-dien-11-one (**1**) was synthesized using a published procedure.³⁴ The ketone (**1**) was then reduced to heneicosa-1,20-dien-11-ol (**2**) using a method similar to that reported.³⁵ The ¹H NMR and ¹³C NMR were in agreement with spectra found previously, and the purity of the compounds was supported by elemental analysis.

11-Fluoroheneicosa-1,20-diene (3). A solution of 5 g (0.031 mol) of diethylaminosulfur trifluoride (DAST) in 25 mL CH₂Cl₂ was cooled to –78 °C and a solution of 5 g (0.016) **2** in 25 mL of CH₂Cl₂ and dry pyridine (2.5 mL) was added dropwise. The mixture was stirred at this temperature for 2 h and then warmed to room temperature and stirred overnight. At this time water was added and the organic phase was extracted with CH₂Cl₂ and then dried with Na₂SO₄ and then the solvent was removed to give a white solid which was purified by chromatography using 97:3 hexanes: ethyl acetate to give 2.85 g (57%) of the product. ¹H NMR (300 MHz CDCl₃): δ 5.82 (m, 2H), 4.97 (m, 4H), 4.54–4.38 (dp, 1H), 2.05 (q, 4H), 1.7–1.2 (bm, 28H). ¹³C NMR (75 MHz, CDCl₃): δ 139.44, 114.35, 64.61, 38.74, 34.03, 29.68, 29.63, 29.39, 29.32, 29.14, 26.71. HRMS: calcd for C₂₁H₃₉F (M⁺), 310.3036; found, 310.3041. Anal. Calcd for C₂₁H₃₉F: C, 81.22; H 12.66; F, 6.12. Found: C, 81.21; H, 12.76; F, 6.03.

11-Chloroheneicosa-1,20-diene (4). To 25 mL of dry pyridine at 0 °C were added 4.5 g (2.4 × 10^{–2} mol) of tosyl chloride and 6.2 g (2.0 × 10^{–2} mol) of heneicosa-1,20-dien-11-ol under argon. The mixture was stirred overnight. After filtration, 200 mL ether was added into the mixture. The mixture was washed with 1 M HCl (50 mL ×3), washed with water (50 mL ×3), dried over MgSO₄, and the solvent was removed under vacuum to yield a crude yellow oil. Purification by chromatography on silica with ether–hexane (15:85) as eluent gave the tosylate which was carried on to the next step. To 150 mL of dry acetone was added 6.8 g (0.16 mol) of LiCl and 5.0 g (0.016 mol) of the 11-tosylheptadeca-1,20-diene under argon. After refluxing for 5 days, the mixture was cooled to room temperature. At this time water was added and the solution was extracted with ether (×3). The organic layer was then washed saturated NaHCO₃ followed by brine and then dried with MgSO₄. After filtration the solvent was removed under vacuum to yield clear oil. The clear oil was purified by flash column chromatography using hexane to yield the desired product as a clear oil (3.7 g, 57%). ¹H NMR (300 MHz CDCl₃): δ 5.79 (m, 2H), 4.79 (m, 4H), 3.86 (m, 1H), 2.02 (q, 4H), 1.69 (m, 4H), 1.50–1.27 (br, 24H). ¹³C NMR (75 MHz, CDCl₃): δ 139.13, 114.12, 64.29, 38.50, 33.80, 29.45, 29.40, 29.16, 29.09, 28.90, 26.48. Anal. Calcd for C₂₁H₃₉Cl: C, 77.14; H 12.02; Cl, 10.84. Found: C, 77.15; H, 12.11; Cl, 10.57.

11-Bromoheneicosa-1,20-diene (5). A solution of heneicosa-1,20-dien-11-ol (**2**) (5 g, 1.6 × 10^{–2} mol) and CBr₄ (6.3 g, 1.9 × 10^{–2} mol) in CH₂Cl₂ (25 mL) was prepared in a 500 mL flask and cooled to 0 °C. Triphenyl phosphine (6.2 g, 2.4 × 10^{–2} mol) was added slowly with stirring. Upon addition of the phosphine, the colorless solution turned a pale brown color and was stirred for an additional 4 h at room temperature. The crude product was

concentrated under reduced pressure and phosphine oxide was recrystallized from diethyl ether at $-20\text{ }^{\circ}\text{C}$. The solution was filtered and the product was purified by flash chromatography using hexane as the eluent to give 5.2 g (88%) of the product as an oil. ^1H NMR (300 MHz CDCl_3): δ 5.80 (m, 2H), 4.95 (m, 4H), 4.01 (m, 1H), 2.05 (q, 4H), 1.78 (m, 4H), 1.50–1.27 (br, 24H). ^{13}C NMR (75 MHz, CDCl_3): δ 139.14, 114.11, 58.87, 39.16, 33.77, 29.41, 29.38, 29.07, 29.03, 28.89, 27.55. HRMS: calcd for $\text{C}_{21}\text{H}_{39}\text{Br}$ (M^+), 370.2235; found, 370.2229. Anal. Calcd for $\text{C}_{21}\text{H}_{39}\text{Br}$: C, 67.90; H 10.58; Br, 21.51. Found: C, 68.01; H, 10.57; Br, 21.21.

General Procedure for Bulk Polymerization. Monomer and Grubbs' first generation catalyst were combined in a ratio of 500:1 under argon atmosphere. The polymerization was conducted at 35–40 $^{\circ}\text{C}$ under vacuum with stirring for 5 days. The reaction was then stopped and 5 mL of toluene was added to dissolve the polymer with stirring. The reaction was allowed to cool to room temperature. The polymers were then precipitated by dripping the toluene solution into cold acidic methanol. They were then isolated by filtration and dried.

General Procedure for Solution Polymerization. The monomer and Grubbs' first generation catalyst (500:1 ratio) were dissolved in CH_2Cl_2 for polymerization of PE19F and in toluene for PE19O under argon and stirred at 35–40 $^{\circ}\text{C}$ for 5 days. The same procedure as described above was used to isolate the polymer.

Polymerization of 11-Fluoroheneicosa-1,20-diene (UPE19F). Synthesized by the solution method as above using 1.0 g (3.2×10^{-3} mol) of **3** and 5.3×10^{-3} g (6.4×10^{-6} mol) of Grubbs' first generation catalyst. Analytical yield. ^1H NMR (300 MHz CDCl_3): δ 5.80 (b, 0.28H), 5.38 (m, 2H), 4.95 (b, 0.70 H), 4.55–4.35 (dp, 1H), 1.95 (m, 4H), 1.65–1.15 (b, 30 H). ^{13}C NMR (75 MHz, CDCl_3): δ 130.64, 130.17, 95.87, 93.65, 35.64, 35.36, 32.85, 29.94, 29.81, 29.80, 29.70, 29.42, 27.51, 25.46, 25.40.

Polymerization of 11-Chloroheneicosa-1,20-diene (UPE19Cl). Synthesized by the bulk method as above using 1.0 g (3.1×10^{-3} mol) of **4** and 5.0×10^{-3} g (6.1×10^{-6} mol) of Grubbs' first generation catalyst. Analytical yield. ^1H NMR (300 MHz CDCl_3): δ 5.80 (b, 0.02H), 5.35 (m, 2H), 4.95 (b, 0.08 H), 3.85 (p, 1H), 1.95 (m, 4H), 1.65 (m, 4H), 1.55–1.15 (b, 24 H). ^{13}C NMR (75 MHz, CDCl_3): δ 130.57, 130.10, 64.56, 38.77, 32.81, 29.96, 29.87, 29.72, 29.66, 29.50, 29.43, 29.36, 27.44, 26.74.

Polymerization of 11-Bromoheneicosa-1,20-diene (UPE19Br). Synthesized by the bulk method as above using 1.0 g (2.7×10^{-3} mol) of **5** and 4.4×10^{-3} g (5.4×10^{-6} mol) of Grubbs' first generation catalyst. Analytical yield. ^1H NMR (300 MHz CDCl_3): δ 5.80 (b, 0.05H), 5.35 (m, 2H), 4.95 (b, 0.14 H), 4.02 (p, 1H), 1.95 (m, 4H), 1.75 (m, 4H), 1.6–1.2 (b, 24 H). ^{13}C NMR (75 MHz, CDCl_3): δ 130.75, 130.29, 59.41, 39.62, 33.01, 30.16, 30.05, 29.89, 29.85, 29.69, 29.55, 29.49, 28.01, 27.63.

General Procedure for Hydrogenation. The polymers containing F or Cl halogens (UPE19F and UPE19Cl) were then hydrogenated using a modified version of the method described by Hahn³⁶ by dissolving in dry *o*-xylene under argon and adding 3.3 equiv of *p*-toluenesulfonyl hydrazide (TSH) and 4 equiv of tri-*n*-propylamine (TPA). The solutions were refluxed for 9 h and then cooled to room temperature. The hydrogenated polymer was precipitated into ice-cold methanol and isolated by filtration. The dried polymer was then redissolved in toluene and reprecipitated by dipping into ice-cold acidic methanol. A white solid was collected by filtration and the polymers were isolated in quantitative yield.

The polymers containing Br halogen (UPE19Br) and ketone (UPE19O) were hydrogenated using a 150 mL Parr high-pressure reaction vessel equipped with a glass liner and Teflon stirbar. Unsaturated polymer (1.0 g) and Wilkinson's catalyst (0.02 g) were added to the glass liner under nitrogen blanket. Finally, 20 mL of toluene were added. The vessel was sealed and attached to a grade 5 hydrogen tank and purged with hydrogen several times. The bomb was charged with 500 psi of H_2 and stirred for 5 days at 80 $^{\circ}\text{C}$. The hydrogenated polymer was dissolved in toluene, and precipitated into methanol. The polymer was then filtered and dried under reduced pressure.

PE19F. Hydrogenation was performed as above. ^1H NMR (300 MHz, toluene- d_8): δ 4.43–4.27 (dm, 1H), 1.7–1.2 (bm, 36H). ^{13}C NMR (75 MHz, toluene- d_8): δ 95.21, 92.96, 36.08, 35.79, 30.30, 30.26, 30.19, 30.16, 25.81, 25.75. M_w (GPC vs PE) = 11 300 g/mol. PDI = (M_w/M_n) = 1.52. Anal. Found: C, 77.62; H, 14.16; F, 5.77.

PE19Cl. Hydrogenation was performed as above. ^1H NMR (300 MHz, CDCl_3): δ 3.86 (p, 1H), 1.68 (m, 4H), 1.55–1.15 (b, 32H). ^{13}C NMR (75 MHz, CDCl_3): δ 64.56, 38.75, 29.92, 29.88, 29.82, 29.75, 29.43, 26.73. M_w (GPC vs PS) = 49 500 g/mol. PDI = (M_w/M_n) = 2.22. Anal. Found: C, 74.98; H, 13.87; Cl, 10.66. A lower molecular weight sample used in the DD/MAS solid-state ^{13}C NMR: M_n (^1H NMR) = 12 000 g/mol.

PE19Br. Hydrogenation was performed as above. ^1H NMR (300 MHz CDCl_3): δ 4.03 (p, 1H), 1.79 (m, 4H), 1.6–1.2 (bm, 32H). ^{13}C NMR (75 MHz, CDCl_3): δ 59.26, 39.42, 29.93, 29.88, 29.82, 29.74, 29.32, 27.82. M_w (GPC vs PS) = 38 100 g/mol. PDI = (M_w/M_n) = 1.72. Anal. Found: C, 60.58; H, 11.43; Br, 19.54.

PE19O. Hydrogenation was performed as described above, and the analytical characterization was consistent with that previously reported in the literature.⁵⁶

Acknowledgment. Funding of this work by the National Science Foundation, Grant Nos. DMR-0503876 and NSF 314110 is gratefully acknowledged. We also gratefully acknowledge Dr. John C. Sworen and Dr. Timothy E. Hopkins for synthetic assistance, URP student Kimberly Thompson for assistance with collection of DSC data, and Dr. Lisa Baugh at Exxon-Mobil for obtaining GPC data for PE19O and PE19F. Generous support from ARO for the acquisition of catalysts is also acknowledged.

References and Notes

- Mathot, V. B. F.; Reynaers, H. Crystallization, Melting and Morphology of Homogeneous Ethylene Copolymers. In *Handbook of Thermal Analysis and Calorimetry*; Cheng, S. Z. D., Ed.; Elsevier: Amsterdam, 2002; Vol. 3, Applications to Polymers and Plastics, p 197.
- Jama, C.; Quensierre, J.-D.; Gengembre, L.; Moineau, V.; Grimblot, J.; Dessaux, O.; Goudmand, P. *Surf. Interface Anal.* **1999**, *27*, 653–658.
- Peacock, A. J. *Handbook of Polyethylene: Structures, Properties, and Applications*; Marcel Dekker: New York, 2000; pp 459–508.
- Anton, D. *Adv. Mater.* **1998**, *10*, 1197–1205.
- Feldman, D.; Barbalata, A. *Synthetic Polymers*; Chapman and Hall: London, 1996; Chapter 2.
- Gottesman, R. T.; Goodman, D. In *Applied Polymer Science*, 2nd ed.; Tess, R. W., Poehlein, G. W., Eds.; American Chemical Society: Washington, DC, 1985; pp 383–440.
- Mathews, G. *PVC: Production, Properties, and Uses*; The Institute of Materials: London, 1996; p 280.
- Yang, H.; Islam, M.; Budde, C.; Rowan, S. J. *J. Polym. Sci., Part A: Polym. Chem.* **2003**, *41*, 2107–2116.
- Walsby, N.; Sundholm, F.; Kallio, T.; Sundholm, G. *J. Polym. Sci., Part A: Polym. Chem.* **2001**, *39*, 3008–3017.
- Tonelli, A. E. *Macromolecules* **1982**, *15*, 290–293.
- Arroyo, N. A.; Hiltner, A. *J. Appl. Polym. Sci.* **1979**, *23*, 1473–1485.
- Endo, K.; Saitoh, M. *Polym. Bull. (Berlin)* **2003**, *49*, 411–416.
- Schilling, F. C.; Tonelli, A. E.; Valenciano, M. *Macromolecules* **1985**, *19*, 356–360.
- Stoeva, S. *J. Appl. Polym. Sci.* **2004**, *94*, 189–196.
- Bowmer, T. N.; Tonelli, A. E. *Polymer* **1985**, *26*, 1195–1201.
- Schwab, P.; Grubbs, R. H.; Ziller, J. W. *J. Am. Chem. Soc.* **1996**, *118*, 100–110.
- Smith, J. A.; Brzezinska, K. R.; Valenti, D. J.; Wagener, K. B. *Macromolecules* **2000**, *33*, 3781–3794.
- Sworen, J. C.; Smith, J. A.; Berg, J. M.; Wagener, K. B. *J. Am. Chem. Soc.* **2004**, *126*, 11238–11246.
- Watson, M. D.; Wagener, K. B. *Macromolecules* **2000**, *33*, 8963–8970.
- Baughman, T. W.; Wagener, K. B. *Adv. Polym. Sci.* **2005**, *176*, 1–42.
- Alamo, R.; Domszy, R.; Mandelkern, L. *J. Phys. Chem.* **1984**, *88*, 6587–6595.
- Alamo, R. G.; Mandelkern, L. *Thermochim. Acta*, **1994**, *238*, 155–201.
- Mandelkern, L. *Crystallization of Polymers*, 2nd ed.; Cambridge University Press: Cambridge, U.K., 2002; Vol. 1.

- (24) Isasi, J. R.; Haigh, J. A.; Graham, J. T.; Mandelkern, L.; Alamo, R. G. *Polymer* **2000**, *41*, 8813–8823.
- (25) Flory, P. J. *Trans. Faraday Soc.* **1955**, *51*, 848–857.
- (26) Crist, B.; Howard, P. R. *Macromolecules* **1999**, *32*, 3057–3067.
- (27) Chen, H. Y.; Chum, S. P.; Hiltner, A.; Baer, E. *J. Polym. Sci., Polym. Phys. Ed.* **2001**, *39*, 1578–1593.
- (28) Stephens, C. H.; Yang, H.; Islam, M.; Chum, S. P.; Rowan, S. J.; Hiltner, A.; Baer, E. *J. Polym. Sci., Polym. Phys. Ed.* **2003**, *41*, 2062–2070.
- (29) Ver Strate, G.; Wilchinsky, Z. W. *J. Polym. Sci., Part A-2* **1971**, *9*, 127–142.
- (30) (a) Wild, L.; Blatz, C. In *New Advances in Polyolefins*, Young, T. C., Ed.; Lenum Press: New York, 1993. (b) Anantawaraskul, S.; Soares, J. B. P.; Wood-Adams, P. M.; Monrabal, B. *Polymer* **2003**, *44*, 2393–2401.
- (31) Wang, W.-J.; Zhu, S. *Macromolecules* **2000**, *33*, 1157–1162.
- (32) Hu, W.; Sirota, E. B. *Macromolecules* **2003**, *36*, 5144–5149.
- (33) Ruiz de Ballesteros, O.; Auriemma, F.; Guerra, G.; Corradini, P. *Macromolecules* **1996**, *29*, 7141–7148.
- (34) Hopkins, T. E.; Wagener, K. B. *Macromolecules* **2003**, *36*, 2206–2214.
- (35) Watson, M. D.; Wagener, K. B. *Macromolecules* **2000**, *33*, 5411–5417.
- (36) Hahn, S. F. *J. Polym. Sci., Part A: Polym. Chem.* **1992**, *30*, 397–408.
- (37) Sworen, J. C.; Smith, J. A.; Wagener, K. B.; Baugh, L. S.; Rucker, S. P. *J. Am. Chem. Soc.* **2003**, *125*, 2228–2240.
- (38) Baughman, T. W.; van der AA, E.; Lehman, S. E.; Wagener, K. B. *Macromolecules* **2005**, *38*, 2550–2551.
- (39) du Toit, F. J.; Sanderson, R. D. *J. Fluorine Chem.* **1999**, *98*, 107–114.
- (40) Bowmer, T. N.; Tonelli, A. E. *J. Polym. Sci., Part B: Polym. Phys.* **1986**, *24*, 1631–1650.
- (41) Hagemann, H.; Snyder, R. G.; Peacock, A. J.; Mandelkern, L. *Macromolecules* **1989**, *22*, 3600–3606.
- (42) Gomez, M. A.; Tonelli, A. E.; Lovinger, A. J.; Schilling, F. C.; Cozine, M. H.; Davis, D. D. *Macromolecules* **1989**, *22*, 4441–4451.
- (43) Gunter, L.; Wegner, G.; Smith, J. A.; Wagener, K. B. *Colloid Polym. Sci.* **2004**, *282*, 773–781.
- (44) Cullity, B. D. *Elements of X-ray Diffraction*; Addison-Wesley: London, 1978.
- (45) Callister, W. D., Jr. *Materials Science and Engineering. An Introduction*; Wiley: New York, 2003.
- (46) Contrasting with the dimension of the “c” axis of orthorhombic crystals, 2.54 Å, the “c” axis of the triclinic cell corresponds to two full repeating units (>40 Å).
- (47) Simanke, A. G.; Alamo, R. G.; Galland, G. B.; Mauler, R. S. *Macromolecules* **2001**, *34*, 6959–6971.
- (48) VanderHart, D. L. *J. Magn. Reson.* **1981**, *44*, 117–125.
- (49) VanderHart, D. L.; Perez, E. *Macromolecules* **1986**, *19*, 1902–1909.
- (50) Alamo, R. G.; VanderHart, D. L.; Nyden, M. R.; Mandelkern, L. *Macromolecules* **2000**, *33*, 6094–6105.
- (51) Zhang, X.; Li, Z.; Yang, H.; Sun, C. *Macromolecules* **2004**, *37*, 7393–7400.
- (52) Hosoda, S.; Nomura, H.; Gotoh, Y.; Kihara, H. *Polymer* **1990**, *31*, 1999–2005.
- (53) Holdsworth, C. D. J.; Hendra, P. J.; Cudby, M. E. A.; Willis, H. A. *Polymer* **1977**, *18*, 1005–1008.
- (54) Roe, R.-J.; Gieniewski, C. *J. Cryst. Growth* **1980**, *48*, 295–302.
- (55) Landes, B. G.; Harrison, I. *Polymer* **1987**, *28*, 911–917.
- (56) Watson, M. D.; Wagener, K. B. *Macromolecules* **2000**, *33*, 3196–3201.

MA0605088